

Relaxation of 2D Turbulence to a Metaequilibrium near the Minimum Enstrophy State

X. -P. Huang and C. F. Driscoll

*Physics Department and Institute for Pure and Applied Physical Sciences,
University of California at San Diego, La Jolla, California 92093*

(Received 30 August 1993)

Relaxation of 2D turbulence has been measured in magnetized electron columns, which follow the same (r, θ) dynamics as 2D incompressible fluids. The turbulence arises from shear instabilities on initially hollow columns, then relaxes to long-lasting, axisymmetric metaequilibria. The measured metaequilibrium vorticity profiles are in close agreement with the minimum enstrophy vortices predicted by the “selective decay” hypothesis.

PACS numbers: 47.27.Jv, 47.32.Cc, 52.25.Wz

Turbulent relaxation processes in two-dimensional (2D), nearly inviscid, incompressible fluids have been actively studied for many years [1], with applications to magnetized plasmas, geophysical flows, and spiral galaxies. An interesting challenge is to predict the relaxed metaequilibrium state (MES) which persists until being damped by viscosity. The “selective decay” theory proposes that 2D turbulence relaxes to the minimum enstrophy state, since fine scale motions strongly dissipate enstrophy while nearly conserving kinetic energy [2–5]. Similar conjectures have been successfully applied to turbulent plasma systems [6]. Other theories assume that the MES is a state of maximum entropy. One approach derives the equilibrium by maximizing the mean-field entropy of a point vortex gas, which serves as an approximation to a real turbulent fluid [7]. A more realistic approach averages over a continuous vorticity distribution, which otherwise conserves all the invariants of inviscid 2D dynamics [8]. The connection between these ideas has been partially explored theoretically [9]; however, to our knowledge, they have not previously been quantitatively tested in experiments.

With low dissipation, simple boundary conditions, and accurate diagnostics, magnetized electron columns provide excellent opportunities to study 2D turbulence. Here, the nondissipative $\mathbf{E} \times \mathbf{B}$ motion in the (r, θ) plane is described by the drift Poisson equations [10],

$$\frac{\partial n}{\partial t} + \mathbf{v} \cdot \nabla n = 0, \quad \mathbf{v} = -\frac{c}{B_z} \nabla \phi \times \hat{\mathbf{z}}, \quad \nabla^2 \phi = 4\pi en, \quad (1)$$

where $\mathbf{v}(r, \theta)$ is the drift velocity, B_z is the axial magnetic field, and $-e$ is the electron charge. The electron density $n(r, \theta)$ is proportional to the flow vorticity ζ , since $\zeta \equiv \hat{\mathbf{z}} \cdot (\nabla \times \mathbf{v}) = (c/B_z) \nabla^2 \phi = (4\pi ec/B_z)n$. The electrostatic potential $\phi(r, \theta)$ is proportional to the stream function, and the nonzero $\partial \phi / \partial r$ at the wall corresponds to free-slip boundary conditions. Consequently, Eqs. (1) are isomorphic to the Euler equation that governs 2D inviscid incompressible fluids. Of course, for fine spatial

scales or long times, plasma “viscosity” not contained in Eqs. (1) must be considered [10,11].

In this paper, we present experimental measurements of freely evolving 2D turbulence in a magnetized electron column bounded by conducting cylindrical walls. An initially hollow column undergoes unstable mode growth, clump formation, turbulent interactions, and relaxation to a metaequilibrium within a few hundred column rotations. We observe that the MES is axisymmetric with a monotonically decreasing density profile, and lasts for about 10^4 rotations. The number of electrons (circulation), angular momentum, and energy are well conserved. Less robust invariants, such as enstrophy and mean-field entropy vary significantly, apparently due to measurement coarse graining or dissipation of small spatial scales intensified by strong mixing. We find that the measured MES density (vorticity) profiles exhibit close agreement with predictions of a minimum enstrophy model, while differing substantially from maximum entropy predictions. We also see small amplitude ($\sim 1.6\%$), shot-to-shot variations in the MES profiles, suggesting that the MES also depends on the dynamical details of the evolution.

The basic geometry of our experimental device is shown in Fig. 1. Electrons from a tungsten filament are contained in a series of conducting cylinders (radius $R_w = 3.05$ cm) enclosed in a vacuum chamber ($\sim 10^{-10}$ torr). The electrons are confined axially by negative voltages ($V_c = -150$ V) on the two end cylinders, and confined radially by a uniform axial magnetic field ($B_z = 507$ G), resulting in a confinement time of about 10 s [10]. A trapped column typically has density $n \leq 1 \times 10^7$ cm $^{-3}$, radius $R_p \sim 2$ cm, axial length $L_p \sim 20$ cm, and electron thermal energy $kT \sim 1$ eV. The electron axial bounce time (~ 1 μ s) is shorter than the column bulk rotation time (~ 10 μ s), and its gyro-radius (~ 50 μ m) is small, allowing the 2D $\mathbf{E} \times \mathbf{B}$ drift approximation.

Experimentally, we first inject and trap a stable quiescent column, then hollow it by temporarily raising V_c toward ground on one end cylinder, allowing electrons from

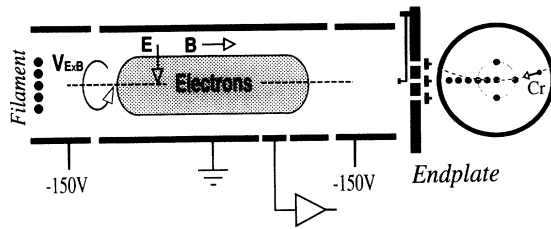


FIG. 1. Schematic of the experimental apparatus, with end-plate collectors viewed from the filament.

the central region to escape. The column then evolves during a hold time t , after which we dump the column axially onto the end-plate collectors shown in Fig. 1. Here, lower-case radial coordinates are normalized to the wall radius, i.e., $r \equiv R/R_w$, with R in cm. A mobile collector Cr (diameter 0.20 cm) can be placed at any radial position, and nine fixed collectors (diameter 0.40 cm) enable angular and radial correlation measurements. The z -averaged electron density $n_i(r, \theta, t)$ is calculated as the number of electrons collected for shot i on a collector positioned at (r, θ) , divided by the collector area and by L_p . We calculate mean densities, fluctuation levels, and spatial correlation functions by ensemble averaging over 1000 shots with nearly identical initial conditions [11], e.g., $n(r, t) \equiv \langle n_i \rangle$ and $\tilde{n}(r, t) \equiv \langle (n_i - n)^2 \rangle^{1/2}$.

An initially hollow density profile, shown as cross symbols in Fig. 2, evolves to the stable, axisymmetric metaequilibrium profile shown as square symbols. The corresponding time evolution of the central mean density $n(0, t)$ and fluctuation level $\tilde{n}(0, t)$ are shown in Fig. 3. The initial evolution is dominated by unstable diocotron modes (Kelvin-Helmholtz shear instabilities) varying as $\cos(l\theta)$ [12]. These diocotron instabilities grow exponentially and saturate with the formation of density clumps

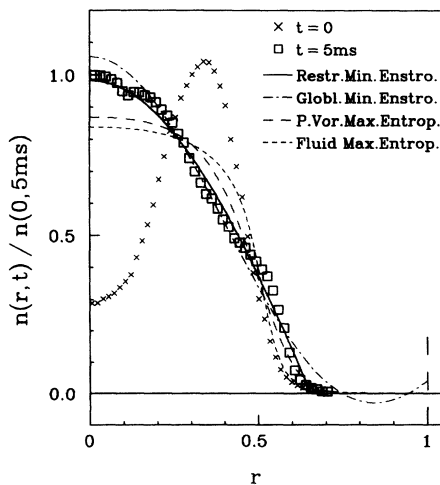


FIG. 2. Measured radial density profiles of the initial and metaequilibrium state, and theoretical predictions from the four models discussed.

[12], as reflected by the rise and peaking of \tilde{n} . Nonlinear turbulent interactions then cause density filamentations, vortex merger, strong mixing, and inward convective transport, resulting in a stable column with monotonically decreasing density profile and a lower fluctuation level [11]. By about 2 ms, the column has relaxed to a low-noise ($\tilde{n}/n \sim 1.6\%$), axisymmetric metaequilibrium state which remains effectively unchanged for 100 ms, i.e., for 10^4 column rotations. In about 1 s, this MES evolves due to “viscosity” from 3D collisions and external asymmetry-induced particle transport [10], which are outside the scope of this paper.

During the relaxation to metaequilibrium, the number of electrons N_L , canonical angular momentum P_θ , and electrostatic energy H_ϕ [10] are well conserved, whereas the entropy S [7] and enstrophy Z_2 [1] vary significantly. These integrals are invariants of the ideal dynamics of Eqs. (1), and are experimentally calculated in scaled form as

$$N_L \equiv R_w^2 \int d^2\mathbf{r} n,$$

$$P_\theta \equiv \int d^2\mathbf{r} (1 - r^2) n/n_0,$$

$$H_\phi \equiv -\frac{1}{2} \int d^2\mathbf{r} (\phi/\phi_0) n/n_0,$$

$$S \equiv - \int d^2\mathbf{r} (n/n_0) \ln(n/n_0),$$

$$Z_m \equiv \frac{1}{m} \int d^2\mathbf{r} (n/n_0)^m,$$

where $m = 2, 3, 4, \dots$. Here, the characteristic density n_0 and potential ϕ_0 are defined as $n_0 \equiv N_L/R_w^2$ and $\phi_0 \equiv eN_L$, calculated at $t = 5$ ms. Note that N_L , P_θ , and H_ϕ are the circulation, angular impulse, and kinetic energy of the $\mathbf{E} \times \mathbf{B}$ drift flow of Eqs. (1).

Table I lists these ideal invariants, as calculated from the measured density profiles at $t = 0, 5$ ms, and 50 ms. Between $t = 0$ and $t = 5$ ms, N_L , P_θ , and H_ϕ drop by 4%

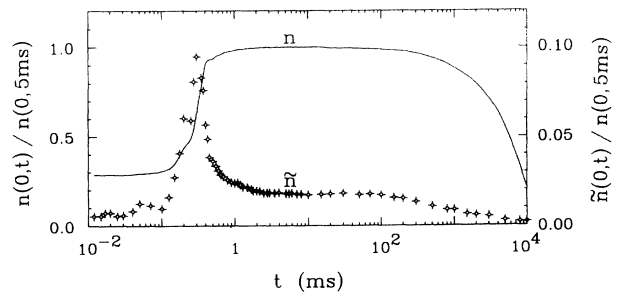


FIG. 3. Temporal evolution of the central mean density $n(0, t)$ and fluctuation level $\tilde{n}(0, t)$.

TABLE I. Measured 2D ideal invariants at various times. Values at 5 ms are absolute; other values (except for S) are expressed as % changes from $t = 5$ ms.

| t | n_{\max} | N_L | P_θ | H_ϕ | Z_2 | Z_3 | S |
|-------|--------------------|--------------------|------------|----------|-------|-------|--------|
| 0 | +4.1% | +1.2% | +1.5% | +3.4% | +22% | +45% | -0.082 |
| 5 ms | 3.05×10^6 | 1.77×10^7 | 0.861 | 0.896 | 0.510 | 0.396 | 0.087 |
| 50 ms | -1.0% | -0.1% | -0.3% | -1.0% | -1.8% | -3.3% | 0.104 |

or less, perhaps largely due to systematic errors such as changes in column end shape. Similarly, the maximum density n_{\max} , which is a local ideal invariant, drops 4% after being transported from $r \simeq 0.4$ to the column center. In contrast, Z_2 and Z_3 fall by more than 20%, and S increases by more than a factor of 2 while changing its sign from negative to positive. All the ideal invariants then remain essentially constant between $t = 5$ ms and 50 ms, indicating that dissipation is negligible for these large spatial scales and intermediate times.

Two variational principles, maximization of entropy and minimization of enstrophy, have been proposed to predict the MES. Maximum entropy profiles from the point vortex model [7] and from the continuous fluid model [8] are calculated numerically from the measured density profile at $t = 0$, and are plotted as dashed curves in Fig. 2. These two profiles are both relatively flat near the column center, apparently due to the assumption of thorough ergodic mixing of the fluid elements. The disagreement with the experimental data suggests that the freely evolving turbulence considered here has not mixed ergodically.

Two minimum enstrophy profiles, from the global model and from a "restricted" model, can be derived analytically [4]. In both models, we solve for the axisymmetric equilibrium profile $n_e(r)$ by minimizing Z_2 subject to constraints that N_L , P_θ , and H_ϕ remain constant. This variational analysis gives

$$\frac{d^2 n_e}{dr^2} + \frac{1}{r} \frac{dn_e}{dr} + \beta^2 (n_e + \gamma) = 0, \quad (2)$$

with the solution $n_e(r) = \alpha J_0(\beta r) - \gamma$, where J_0 is the zeroth order Bessel function. The parameters (α, β, γ) and the minimum enstrophy Z_2^{\min} are obtained from (N_L, P_θ, H_ϕ) . For the global minimum enstrophy model, we use $n_e(r)$ in the entire region of $0 \leq r \leq 1$. This profile, shown as the dash-dotted curve in Fig. 2, typically goes negative near the wall and is not monotonically decreasing. Clearly, negative density would be unphysical, and nonmonotonic profiles are generally unstable to diocotron instabilities.

In our restricted minimum enstrophy model, $n_e(r)$ follows the solution of Eq. (2) until it reaches zero at some radius r_0 , after which $n_e = 0$. This yields a solution

$$n_e(r) = \begin{cases} \alpha [J_0(\beta r) - J_0(\beta r_0)], & 0 \leq r \leq r_0, \\ 0, & r_0 < r \leq 1, \end{cases} \quad (3)$$

where (α, β, r_0) and Z_2^{\min} are again determined from the

measured (N_L, P_θ, H_ϕ) , with no adjustable parameters. This prediction, plotted as the solid curve in Fig. 2, is close to the experimentally measured metaequilibrium density profile, supporting the "selective decay" hypothesis [2-5].

In this restricted model, the explicit P_θ dependence can be eliminated [11]. The rescaled minimum enstrophy $\hat{Z}_2^{\min} \equiv 4\pi(1 - P_\theta)Z_2^{\min}$ is then only a function of excess energy $H_\phi^{\text{exc}} \equiv H_\phi - H_\phi^{\min}$. Here, $H_\phi^{\min} = \{1/2 - \ln[2(1 - P_\theta)]\}/2$ is the minimum energy possible for a column with given N_L and P_θ , which occurs for a uniform density profile. The solid curve in Fig. 4 shows the predicted \hat{Z}_2^{\min} versus H_ϕ^{exc} . At $H_\phi^{\text{exc}} = 0$, the minimum enstrophy state is a uniform density column of radius $r_0 = [2(1 - P_\theta)]^{1/2}$, with $\hat{Z}_2^{\min} = 1$. For $H_\phi^{\text{exc}} \geq [5/12 - \ln(3/2)]/2 = 5.6 \times 10^{-3}$, the "temperature" of this state is negative, in analogy with the maximum entropy analysis [7]. As H_ϕ^{exc} approaches $H_u \equiv [12/j_{1,1}^2 + \ln(1 - 8/j_{1,1}^2)]/2 = 1.5 \times 10^{-2}$, off-axis states with slightly lower enstrophy may exist [13]. Finally, for $H_\phi^{\text{exc}} > H_u$, analytic solution of Eq. (3) is not possible [11].

We have experimentally measured the relaxed metaequilibrium states resulting from initially hollow columns of various diameters, "hollowness" depths, and axial lengths, in several magnetic fields. The measured MES profiles give rescaled enstrophy \hat{Z}_2 versus H_ϕ^{exc} , plotted as circles in Fig. 4. Here, the specific evolution of Figs. 2 and 3 is shown by the solid symbols: The rescaled en-

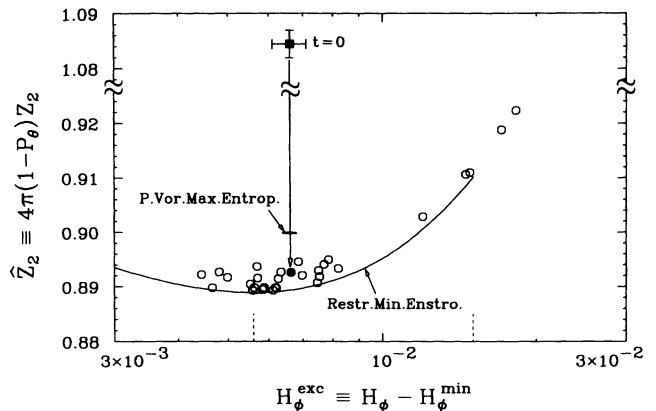


FIG. 4. The rescaled enstrophy \hat{Z}_2 of the metaequilibrium state versus excess energy H_ϕ^{exc} , from measurements (circles) and from the restricted minimum enstrophy model (curve).

strophy varies from $\hat{Z}_2 = 1.084$ at $t = 0$ to $\hat{Z}_2 = 0.892$ at $t = 5$ ms, with the restricted minimum enstrophy prediction being $\hat{Z}_2^{\min} = 0.890$. For comparison, the point vortex maximum entropy profile would have $\hat{Z}_2 = 0.900$. The measured enstrophy of the MES is close to the prediction of the restricted minimum enstrophy theory for each initial condition, typically within 1%–2% of the enstrophy available for dissipation. This reflects the fact that the measured $n(r)$ profiles agree well with Eq. (3), comparable or better than the MES shown in Fig. 2.

The measured 1.6% fluctuation level of the MES in Fig. 3 is typical of these evolutions, and reflects shot-to-shot variations in the radial density profile. At $t = 5$ ms, there are essentially no angular variations: two-point correlations between the four collectors at $r = 0.36$ (see Fig. 1) are about 0.90, indicating that any remaining θ variations are less than 0.2% of the mean density at that radius. Structured radial correlations are also observed in the MES profile, which apparently reflects the requirements that N_L , P_θ , and H_ϕ are constant from shot to shot [11]. We also note that this 1.6% radial profile variation level is about 4 times greater than the variations in the initial condition from which they presumably arise. This suggests that the details of the turbulent evolution affect the MES profile; however, these effects are small compared to the differences between the measured and predicted MES profiles. Experimentally, there is one caveat: If the $l = 1$ (center-of-mass) mode is not carefully removed from the initial condition, it will remain indefinitely and dominate the late time fluctuation measurements.

Some unstable initial conditions, such as two merging vortices [14], have $H_\phi^{\text{exc}} > H_u$, and the measured MES profiles are not describable by Eq. (3). Further theory may establish what the general minimum enstrophy states are, and further experiments may determine when unstable initial conditions *do* relax to these states.

Finally, we note that these experiments may model the emergence of coherent vortices from a region of nonzero net circulation within a larger field of turbulence with vanishing total circulation [15]. Of course, our cylindrical walls give complete isolation of this region, whereas in a turbulent flow other regions may perturb any given vortex, with merger of like-signed vortices being perhaps

the most extreme case.

We gratefully acknowledge theory contributions by R. A. Smith and experimental suggestions by the late J. H. Malmberg. We also thank T. M. O'Neil, D. H. E. Dubin, and K. S. Fine for helpful discussions. This research is supported by the U.S. Department of Energy (DE-FG03-85ER53199), the National Science Foundation (PHY91-20240), and the Office of Naval Research (N00014-89-J-1714).

-
- [1] G. K. Batchelor, *Phys. Fluids Suppl. II* **12**, 233 (1969); R. H. Kraichnan and D. Montgomery, *Rep. Prog. Phys.* **43**, 547 (1980).
 - [2] F. P. Bretherton and D. B. Haidvogel, *J. Fluids Mech.* **78**, 129 (1976).
 - [3] W. H. Matthaeus and D. Montgomery, *Ann. N.Y. Acad. Sci.* **357**, 203 (1980).
 - [4] C. E. Leith, *Phys. Fluids* **27**, 1388 (1984).
 - [5] A. Hasegawa, *Adv. Phys.* **34**, 1 (1985).
 - [6] J. B. Taylor, *Rev. Mod. Phys.* **58**, 741 (1986).
 - [7] L. Onsager, *Nuovo Cimento Suppl.* **6**, 279 (1949); G. Joyce and D. Montgomery, *J. Plasma Phys.* **10**, 107 (1973); R. A. Smith, *Phys. Rev. A* **43**, 1126 (1991).
 - [8] D. Lynden-Bell, *Mon. Not. R. Astron. Soc.* **136**, 101 (1967); J. Sommeria, C. Staquet, and R. Robert, *J. Fluid Mech.* **233**, 661 (1991); J. Miller, P. B. Weichman, and M. C. Cross, *Phys. Rev. A* **45**, 2328 (1992).
 - [9] T. H. Dupree, *Phys. Fluids B* **4**, 3102 (1992).
 - [10] *Non-Neutral Plasma Physics*, edited by C. W. Roberson and C. F. Driscoll, AIP Conf. Proc. No. 175 (AIP, New York, 1988), pp. 1–74.
 - [11] X. -P. Huang, Ph.D. thesis, University of California at San Diego, 1993.
 - [12] C. F. Driscoll *et al.*, *Plasma Physics and Controlled Nuclear Fusion Research 1988* (IAEA, Vienna, 1989), Vol. 3, p. 507; C. F. Driscoll and K. S. Fine, *Phys. Fluids B* **2**, 1359 (1990).
 - [13] R. A. Smith and T. M. O'Neil, *Phys. Fluids B* **2**, 2961 (1990).
 - [14] K. S. Fine *et al.*, *Phys. Rev. Lett.* **67**, 588 (1991); T. B. Mitchell, C. F. Driscoll, and K. S. Fine, *Phys. Rev. Lett.* **71**, 1371 (1993).
 - [15] J. C. McWilliams, *J. Fluid Mech.* **146**, 21 (1984); D. Montgomery *et al.*, *Phys. Fluids A* **4**, 3 (1992).

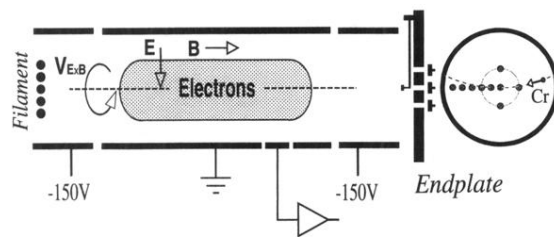


FIG. 1. Schematic of the experimental apparatus, with end-plate collectors viewed from the filament.